Secondary Structure of Myristoylated Recoverin Determined by Three-Dimensional Heteronuclear NMR: Implications for the Calcium–Myristoyl Switch†

James B. Ames,‡ Toshiyuki Tanaka,§ Lubert Stryer,‡ and Mitsuhiko Ikura*,§

Department of Neurobiology, Stanford University School of Medicine, Stanford, California 94305, and Division of Molecular and Structural Biology, Ontario Cancer Institute, and Department of Medical Biophysics, University of Toronto, 500 Sherbourne Street, Toronto, Ontario, Canada M4X 1K9

Received April 19, 1994; Revised Manuscript Received June 27, 1994®

ABSTRACT: Recoverin, a new member of the EF-hand superfamily, serves as a Ca^{2+} sensor in vision. A myristoyl or related *N*-acyl group is covalently attached at its N-terminus and plays an essential role in Ca^{2+}-dependent membrane targeting by a novel calcium–myristoyl switch mechanism. The structure of unmyristoylated recoverin containing a single bound Ca^{2+} has recently been solved by X-ray crystallography [Flaherty, K. M., Zozulya, S., Stryer, L., & McKay, D. B. (1993) *Cell 75*, 709–716]. We report here multidimensional heteronuclear NMR studies on Ca^{2+}-free, myristoylated recoverin (201 residues, 23 kDa). Complete polypeptide backbone ^1H, ^{15}N, and ^{13}C resonance assignments and secondary structure are presented. We find 11 helical segments and two pairs of antiparallel β-sheets, in accord with the four EF-hands seen in the crystal structure. The present NMR study also reveals some distinct structural features of the Ca^{2+}-free myristoylated protein. The N-terminal helix of EF-2 is flexible in the myristoylated Ca^{2+}-free protein, whereas it has a well-defined structure in the unmyristoylated Ca^{2+}-bound form. This difference suggests that the binding of Ca^{2+} to EF-3 induces EF-2 to adopt a conformation favorable for the binding of a second Ca^{2+} to recoverin. Furthermore, the N-terminal helix (K5–E16) of myristoylated Ca^{2+}-free recoverin is significantly longer than that seen in the unmyristoylated Ca^{2+}-bound protein. We propose that this helix is stabilized by the attached myristoyl group and may play a role in sequestering the myristoyl group within the protein in the Ca^{2+}-free state.

Recoverin is a 23-kDa calcium-binding protein in retinal rod and cone cells. It was discovered in the search for a soluble calcium-sensitive activator of photoreceptor guanylate cyclase (Dizhoor et al., 1991; Lambrecht & Koch, 1991) and was also identified as the antigen in cancer-associated retinopathy (Polans et al., 1991). Subsequent studies showed that calcium-bound recoverin has a different role: it prolongs the photoresponse (Gray-Keller et al., 1993; Lagnado et al., 1994), most likely by blocking the phosphorylation of photoexcited rhodopsin (Kawamura, 1993). This effect of recoverin is reversed by the light-induced lowering of the calcium level. The shortened lifetime of photoexcited recoverin at low calcium concentration promotes recovery of the dark state and contributes to adaptation to background light.

Interest in recoverin has been heightened by the finding that the retinal protein contains a covalently attached myristoyl group at its amino terminus (Dizhoor et al., 1992). Also, Ca^{2+} binding causes recoverin to partition into lipid bilayers (Dizhoor et al., 1993; Zozulya & Stryer, 1992), suggesting that the myristoyl group may play an active role in the function of recoverin and that the molecule has a "calcium–myristoyl switch" mechanism. Myristoyl switches are now being found in an increasing number of signal transduction proteins including all Src family members (Resh, 1994) and appear to serve a common mechanism of membrane targeting. Recoverin is a member of an emerging branch of the EF-hand superfamily (McPhalen et al., 1991; Moncrief et al., 1990; Persechini et al., 1989; Strynadka & James, 1989), which includes S-modulin from frog rods (Kawamura et al., 1992), visinin from chicken cones (Yamagata et al., 1990), several neurocalcins and hippocalcin from mammalian brain (Kobayashi et al., 1992; Kuno et al., 1992; Lenz et al., 1992; Okazaki et al., 1992; Takamatsu et al., 1992; Terasawa et al., 1992), and frequenin from *Drosophila* synapses (Pongs et al., 1993). These proteins are more than 45% identical in amino acid sequence and hence are likely to be structurally and functionally similar. They differ from calmodulin and troponin C in having additional residues at the amino and carboxy termini, plus an insertion between the third and fourth EF-hand domains. Also, the recoverin family of proteins all appear to exhibit a calcium–myristoyl switch for membrane targeting not found in calmodulin or troponin C.

The crystallographic structure of unmyristoylated recoverin with one Ca^{2+} bound was recently solved at 1.9-Å resolution (Flaherty et al., 1993). Recoverin contains 4 EF-hand domains (referred to as EF-1, EF-2, EF-3, and EF-4, in the N- to C-terminal direction), 29-residue helix–loop–helix motifs found in parvalbumin, troponin C, calmodulin, and other members of the superfamily (Moncrief et al., 1990). Recoverin's four EF-hand domains are arranged in a compact, linear array in contrast to the dumbbell arrangement seen in the crystal structures of calmodulin (Babu et al., 1988; Kretsinger et al., 1986) and troponin C (Herzberg & James,

† This work was supported by grants from the National Institutes of Health (GM24032 and EY02005) to L.S. and in part by grants to M.I. from the Medical Research Council of Canada and the Human Frontier Science Program Organization. J.B.A. is supported by an NIH Postdoctoral Fellowship (EY06418-02) and T.T. by an Ontario Cancer Institute/Amgen postdoctoral fellowship. M.I. is a recipient of a Medical Research Council of Canada Scholarship.

* To whom correspondence should be addressed.
‡ Stanford University.
§ Ontario Cancer Institute.

® Abstract published in *Advance ACS Abstracts,* August 1, 1994.

0006-2960/94/0433-10743$04.50/0

1988). Ca^{2+} only binds to EF-3 in the crystal form of recoverin; however, Sm^{3+} is found to bind to both EF-2 and EF-3. Another notable feature of the crystal structure is an unusual concave hydrophobic surface formed by nonpolar residues from EF-1 and EF-2. This raises the attractive hypothesis that these exposed nonpolar residues form a binding site for the covalently attached myristoyl group or for a target protein. It is interesting to ask whether the binding of Ca^{2+} changes the conformation and interactions of this hydrophobic region as part of the Ca^{2+}–myristoyl switch mechanism. To gain further insights into the molecular mechanism of the Ca^{2+}–myristoyl switch, the structure of myristoylated recoverin as a function of Ca^{2+} concentration needs to be determined. Since the myristoylated protein in both Ca^{2+}-free and Ca^{2+}-bound states has not formed suitable crystals for X-ray crystallography, the structure of these forms must be studied by other means.

The recent availability of recombinant myristoylated recoverin (Ray et al., 1992) makes it possible to determine the atomic resolution structure of the myristoylated protein using multidimensional $^1H/^{13}C/^{15}N$ triple-resonance NMR techniques. Herein we report the sequence-specific assignments of ^1H, ^{13}C, and ^{15}N NMR signals of myristoylated recoverin in the Ca^{2+}-free state. The secondary structure of myristoylated recoverin has been deduced on the basis of these resonance assignments, together with the analysis of NOE,[1] $^3J_{NH\alpha}$ coupling constants, backbone amide hydrogen exchange rates, and chemical shifts. The results are compared with the recent crystal structure of Ca^{2+}-bound unmyristoylated recoverin.

MATERIALS AND METHODS

Sample Preparation. Recombinant myristoylated recoverin was produced by coexpressing recoverin and *N*-myristoyl-CoA transferase in *E. coli* (Ray et al., 1992). Uniformly ^{15}N- and $^{15}N/^{13}C$-labeled proteins with a nonlabeled myristoyl group covalently attached to the N-terminus were obtained by growing *E. coli* cells carrying pTrec2 and pBB131 plasmids in M9 minimal medium (Sambrook et al., 1989) supplemented with $MgSO_4$ (0.5 mM), ampicillin (0.1 mg/mL), kanamycin (0.1 mg/mL), and thiamine (1 mg/L) and using $^{15}NH_4Cl$ and [$^{13}C_6$]-D-glucose as the sole nitrogen and carbon sources. Myristic acid (5 mg/L) was added to the medium ~2 h before the induction of *N*-myristoyl-CoA transferase. Myristoylated recoverin was purified using phenyl-Sepharose CL-4B (Pharmacia) and Q-Sepharose (Pharmacia) fast-flow column chromatography (Zozulya & Stryer, 1992). Typically, 10 mg of labeled protein, with >95% $^{15}N/^{13}C$ enrichment, was obtained from 1 L of culture. The purified protein was placed in 50 mM NH_4HCO_3 (pH 8.0) using a Sephadex G-25M (Pharmacia PD-10) desalting column and then lyophilized to remove all solutes from the purification procedure. Samples for NMR experiments were prepared by dissolving lyophilized protein (1 mM) in 95% H_2O/5% ^2H_2O containing 0.1 M KCl, 10 mM [$^2H_{10}$]DTT, and 1 mM [$^2H_{12}$]EDTA. The pH was adjusted to 6.8 using dilute (4%) NaO^2H or ^2HCl without correction for isotope effects.

NMR Spectroscopy. NMR experiments were performed, unless otherwise noted, on a UNITY-plus 500 spectrometer equipped with a four-channel NMR interface and a triple-resonance probe with an activity shielded *z* gradient, together with a pulse field gradient (PFG) accessory. Pulse field gradients were employed to eliminate artifacts and minimize the intense water signal (Bax & Pochapsky, 1992). In addition, gradients were used to select for the coherent-transfer pathway passing through ^{15}N in all 2D and 3D experiments [except HA(CACO)NH] for which the amide proton was detected (Kay et al., 1992).

The 2D ^{15}N–^1H HSQC (Bodenhausen & Ruben, 1980; Bax et al., 1990) spectrum (Figure 1) was recorded using the enhanced sensitivity method of Kay et al. (1992). The number of complex points and acquisition times were as follows: ^{15}N (F_1) 300, 180 ms, ^1H (F_2) 512, 77 ms, 64 transients. The HMQC-J (Kay & Bax, 1990) spectrum was recorded on a UNITY-600 spectrometer with the following numbers of complex points and acquisition times: ^{15}N (F_1) 300, 180 ms, ^1H (F_2) 512, 64 ms, 272 transients.

Slowly exchanging amide protons were identified by recording a series of gradient-enhanced ^{15}N–^1H HSQC (Kay et al., 1992) experiments at a range of time intervals (5, 37, 74, 238, 368, 668, 1088 min) beginning immediately after dissolving lyophilized protein in ^2H_2O. The spectra were recorded with the following numbers of complex points and acquisition times: ^{15}N (F_1) 128, 64 ms, ^1H (F_2) 512, 77 ms. The first two HSQC spectra were recorded with 8 transients (total measurement time 32 min), the following three HSQC spectra with 16 transients, and the last two HSQC spectra with 32 transients.

The $^{15}N\{^1H\}$ NOE was measured as described (Kay et al., 1989). Three sets of spectra with and without the NOE effect were recorded with the following numbers of complex points and acquisition times: ^{15}N (F_1) 256, 128 ms, ^1H (F_2) 1024, 64 ms, 16 transients. Resonance intensities were used to determine the NOE values, and the average values of three experiments were calculated.

Two ^{15}N-edited NOESY-HMQC (Zuiderweg & Fesik, 1989; Marion et al., 1989b) spectra were recorded on the uniformly ^{15}N-labeled H_2O sample with an NOE mixing time of 100 ms: one with water presaturation on a UNITY-600 spectrometer and one with the gradient-enhanced method (Kay et al., 1992) on a UNITY-plus 500. The following numbers of complex points and acquisition times were used for both cases: ^1H (F_1) 128, 19.7 ms, ^{15}N (F_2) 28, 24 ms, ^1H (F_3) 512, 64 ms (16 transients).

All triple-resonance 3D spectra were recorded on the uniformly $^{15}N/^{13}C$-labeled H_2O sample with the following numbers of complex points and acquistion times: HNCO (Kay et al., 1990), ^{15}N (F_1) 28, 24 ms, ^{13}CO (F_2) 64, 42.7 ms, ^1H (F_3) 512, 64 ms (16 transients); HNCA (Kay et al., 1990), ^{15}N (F_1) 28, 24 ms, $^{13}C_\alpha$ (F_2) 32, 10 ms, ^1H (F_3) 512, 64 ms (64 transients); HA(CACO)NH (L. E. Kay, personal communication), ^{15}N (F_1) 28, 24 ms, $^1H_\alpha$ (F_2) 48, 19.2 ms, ^1H (F_3) 512, 64 ms (64 transients); HNCAHA (Kay et al., 1991), ^{15}N (F_1) 28, 24 ms, $^1H_\alpha$ (F_2) 48, 19.2 ms, ^1H (F_3) 512, 64 ms (64 transients); HNCACB (Wittekind & Mueller, 1993), $^{13}C_{\alpha/\beta}$ (F_1) 38, 5 ms, ^{15}N (F_2) 28, 24 ms, ^1H (F_3) 512, 64 ms (64 transients); CBCA(CO)NH (Grzesiek & Bax, 1992),

[1] Abbreviations: CBCA(CO)NH, β-proton to α/β-carbon (via carbonyl carbon) to nitrogen to amide proton correlation; DTT, dithiothreitol; *E. coli*, *Escherichia coli*; EDTA, ethylenediaminetetraacetic acid; HNCAHA, H_α proton (via C_α carbon) to nitrogen to amide proton correlation; HA(CACO)NH, H_α proton (via C_α and carbonyl carbon) to nitrogen to amide proton correlation; (HB)CBCACO(CA)HA, C_α and C_β carbons to carbonyl carbon (via C_α carbon) to H_α proton correlation; HCCH-TOCSY, proton–carbon–proton correlation using carbon total correlated spectroscopy; HMQC, heteronuclear multiple quantum correlation; HNCO, amide proton to nitrogen to carbonyl carbon correlation; HNCA, amide proton to nitrogen to α-carbon correlation; HNCACB, amide proton to nitrogen to α/β-carbon correlation; HSQC, heteronuclear single quantum correlation; NOESY, nuclear Overhauser effect spectroscopy; NOE, nuclear Overhauser effect; PFG, pulse field gradient.

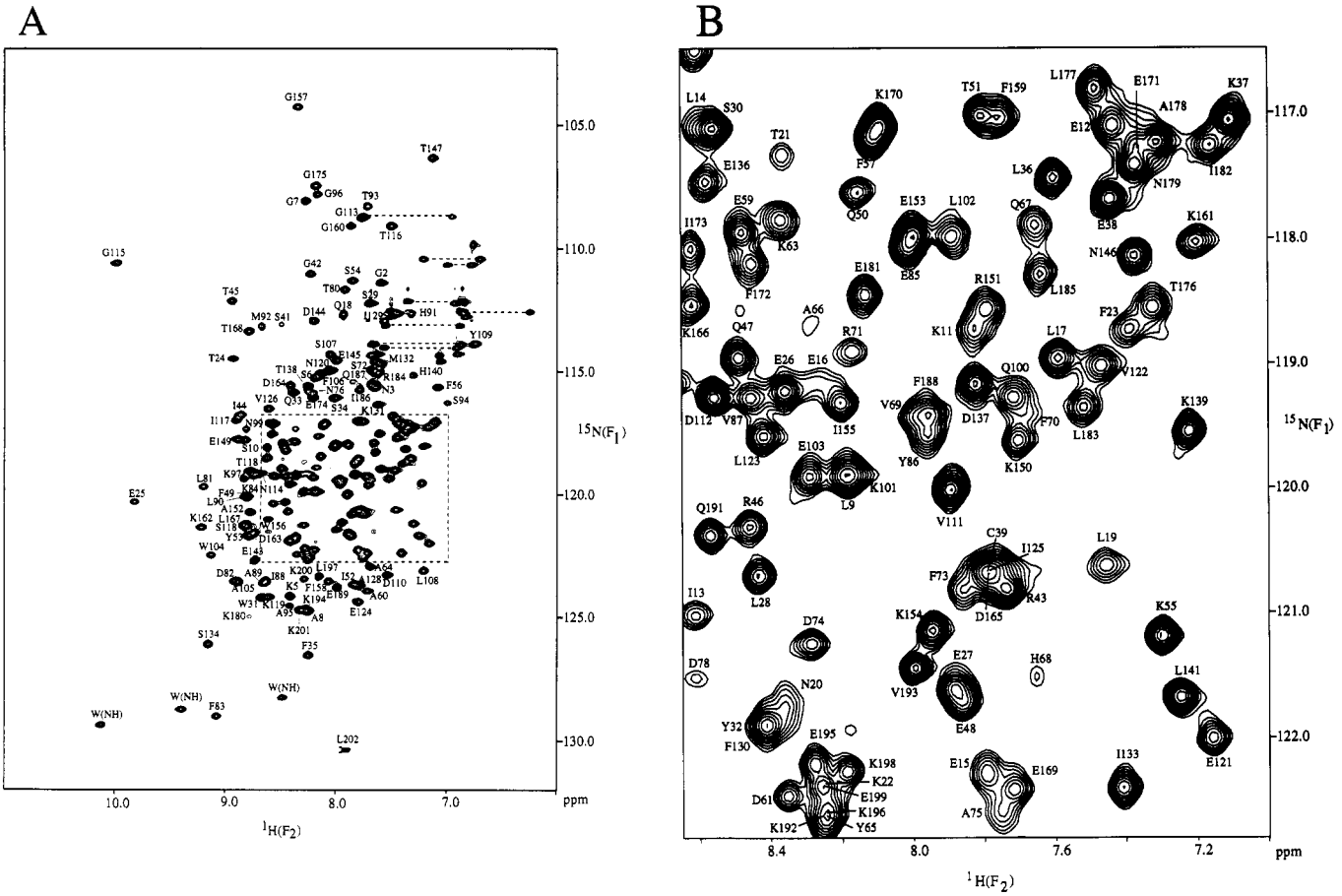

FIGURE 1: (A) 2D ^{15}N–^{1}H HSQC spectrum of Ca^{2+}-free myristoylated recoverin, uniformly labeled with ^{15}N (>95%); and (B) expanded view of region inside dotted lines of the 2D ^{15}N–^{1}H HSQC spectrum, recorded at 500-MHz ^{1}H frequency. Cross peaks connected by dotted lines correspond to Gln and Asn side-chain NH_2 groups. Indole NH cross peaks from Trp side chains are marked as W(NH).

$^{13}C_{\alpha/\beta}$ (F_1) 38, 5 ms, ^{15}N (F_2) 28, 24 ms, ^{1}H (F_3) 512, 64 ms (32 transients); (HB)CBCACO(CA)HA (Kay, 1993), $^{13}C_{\alpha/\beta}$ (F_1) 52, 7.1 ms, ^{13}CO (F_2) 64, 42 ms, ^{1}H (F_3) 384, 64 ms (16 transients).

Two gradient-enhanced HCCH-TOCSY (Bax et al., 1990; Kay et al., 1993) spectra (with mixing times of 7 and 14 ms, respectively) were recorded with the following number of complex points and acquisition times: ^{1}H (F_1) 128, 28.4 ms, ^{13}C (F_2) 32, 8.9 ms, ^{1}H (F_3) 512, 64 ms (16 transients). Simultaneous $^{15}N/^{13}C$-edited NOESY-HSQC (Pascal et al., 1994) spectra with a mixing time of 100 ms were recorded with the following number of complex points and acquisition times: ^{1}H (F_1) 128, 25.6 ms, $^{13}C/^{15}N$ (F_2) 32, 10.7 ms, ^{1}H (F_3) 512, 64 ms.

All data sets were processed on Sun Sparc2 and Sparc10 workstations using a combination of software written at the National Institutes of Health and commercial software (NMRZ, New Methods Research Inc., Syracuse, NY). The programs nmrPipe and nmrDraw (F. Delaglio, unpublished) were used for 3D NMR data processing and display. The programs Capp and Pipp (Garrett et al., 1991) were used for peak picking and spectral analysis. Where necessary, the residual water signal in spectra was removed using a time-domain deconvolution approach developed by Marion et al. (1989a). In the case of gradient-enhanced HCCH-TOCSY and simultaneous $^{15}N/^{13}C$-edited NOESY-HSQC, the residual water signal was eliminated using a low-order polynomial fit of the data (Muhandiran et al., 1993). Further details of data processing were the same as described previously (Bagby et al., 1994).

RESULTS

1D and 2D NMR Experiments. Recombinant myristoylated recoverin has been obtained using an *E. coli* overex-

Table 1: Summary of Nuclei Correlated in Triple-Resonance 3D NMR Experiments

pair of experiments	correlation type	no. of correlations[a]	linkage type[b]	linkage no.
CBCA(CO)NH	$HN(i)$–$N(i)$–$C_\alpha/C_\beta(i-1)$	354	C_α/C_β	155[c]
HNCACB	$HN(i)$–$N(i)$–$C_\alpha/C_\beta(i)$	339		
HNCO	$HN(i)$–$N(i)$–$CO(i-1)$	241	CO	165
(HB)CBCACO(CA)HA	$H_\alpha(i)$–$CO(i)$–$C_\alpha/C_\beta(i)$	407		
HA(CACO)NH	$HN(i)$–$N(i)$–$H_\alpha(i-1)$	165	H_α	163
HNCAHA	$HN(i)$–$N(i)$–$H_\alpha(i)$	190		

[a] Number of correlations for each experiment is given by the total number of peaks obtained using the Capp and Pipp programs (Garrett et al., 1991). [b] The type of nuclei through which spin systems of adjacent residues are connected by the pair of experiments. [c] Includes the number of linkages through C_α or C_β.

pression system which coexpresses recoverin and myristoyl-CoA transferase (Ray et al., 1992). The protein was labeled with ^{15}N and ^{13}C while the myristoyl group was not labeled. We recorded several 1D spectra on uniformly ^{15}N-labeled myristoylated recoverin in 95% H_2O/5% ^2H_2O (containing 0.1 M KCl) under various conditions: 0–10 mM DTT, 0–5 mM $CaCl_2$, pH 6.8–7.3, at 25–37 °C. NMR spectra of monomeric recoverin could only be observed for the Ca^{2+}-free state. When stoichiometric amounts of Ca^{2+} were added, the NMR linewidths became very broad, presumably due to protein aggregation caused by the exposed myristoyl group (Kataoka et al., 1993). DTT (10 mM) was required to prevent the Ca^{2+}-free protein from precipitating during the NMR experiment. Also, the protein tended to precipitate at temperatures above 30 °C. Approximately ten amide proton peaks disappeared from the spectrum when the pH was elevated from 6.8 to 7.3 due to rapid exchange. Thus, we chose to study the NMR spectra of the Ca^{2+}-free form of myristoylated recoverin under the following conditions: 1 mM myristoylated recoverin in 0.1 M KCl, 10 mM [$^2H_{10}$]DTT, 1 mM [$^2H_{12}$]EDTA, pH 6.8 at 30 °C.

A ^{15}N–^1H HSQC spectrum of uniformly ^{15}N-labeled recoverin is shown in Figure 1A. At pH 6.8, a total of 228 peaks are evident. We expect 194 main-chain amide ^1H peaks (201 residues minus 7 prolines) and ~50 side-chain NH peaks. Most of the peaks are well resolved due to marked dispersion of ^{15}N and ^1H chemical shifts. However, some of the resonances are overlapped. Figure 1B shows an expanded view of the most crowded region of the 2D ^{15}N–^1H HSQC spectrum. It is possible by visual inspection to resolve most of the overlapping components. In a few cases, however, the components cannot be distinguished. For example, the large unresolved peak near the ^{15}N shift (F_2) of 120.6 ppm and ^1H (F_1) shift of 7.8 ppm actually consists of five components: C39, R43, F73, I125, and D165. These components are readily resolved in triple-resonance 3D experiments described below that correlate the amide ^{15}N and ^1H with backbone ^{13}C resonances.

Sequence-Specific Resonance Assignments. The sequential assignment procedure used for recoverin is similar to those reported previously (Archer et al., 1993; Byeon et al., 1993; Metzler et al., 1993; Bagby et al., 1994), except that we have added a recently reported triple-resonance 3D experiment referred to as (HB)CBCACO(CA)HA (Kay, 1993). This additional experiment provided unambiguous, independent junction points between adjacent amino acid residues through ^{13}CO frequencies and proved to be crucial for completing the assignments of recoverin. In addition, experiments were recorded using pulse field gradients to eliminate the intense water signal which helped to enhance correlations from fast exchanging amide protons whose cross peak intensities are often more attenuated in standard ^{15}N–^1H HSQC spectra with water presaturation. It should be noted that complete backbone assignments were obtained using two H_2O samples: one with uniformly ^{15}N-labeled and the other with ^{13}C/^{15}N-labeled protein.

The initial step in making backbone assignments is the construction of amino acid spin systems at the dipeptide level using the CBCA(CO)NH, HNCACB, HA(CACO)NH, HNCAHA, CA(CO)NH, and HNCA spectra. The cross peaks in these data correlate $^1H_\alpha$, $^{13}C_\alpha$, or $^{13}C_\beta$ of residues ($i-1$) and i with amide $^1H(i)$ and $^{15}N(i)$ chemical shift pairs within a specified tolerance (typically ^1H ±0.03, ^{15}N ±0.3 ppm). Table 1 summarizes the total numbers of cross peaks obtained from these triple-resonance spectra using computer programs together with manual inspection of the chemical shift tables and the 3D spectra. At this stage, the amino acid type for a number of amide ^1H and ^{15}N chemical shift pairs was determined on the basis of the characteristic $^{13}C_\alpha$, $^{13}C_\beta$, $^1H_\alpha$, and $^1H_\beta$ shifts (Howarth & Lilley, 1978; Grzesiek & Bax, 1993). Glycine, alanine, serine, and threonine were most easily identified. However, the assignment table was incomplete at this stage because of resonance overlap in the amide ^1H and ^{15}N frequencies and a lack of $^{13}C_\alpha(i)$ and $^{13}C_\beta(i)$ shifts due to the low sensitivity of the HNCACB experiment.

The second step is to sequentially assign the amide ^1H and ^{15}N chemical shift pairs associated with all or some of $^{13}C_\alpha(i-1)$, $^{13}C_\beta(i-1)$, $^1H_\alpha(i-1)$, $^{13}CO(i-1)$, $^{13}C_\alpha(i)$, $^{13}C_\beta(i)$, $^1H_\alpha(i)$, and $^{13}CO(i)$ chemical shifts. This was achieved by matching the intraresidue $^{13}C_\alpha$, $^{13}C_\beta$, ^{13}CO, and $^1H_\alpha$ shifts of a given amide ^1H/^{15}N chemical shift pair with the interresidue shifts of another amide ^1H/^{15}N pair. This resulted in many stretches of amino acid spin systems ranging from dipeptide fragments to stretches of as many as 20 residues. In addition, amide ^1H/^{15}N chemical shift pairs were linked together on the basis of sequential NOE connectivities such as $d_{NN(i,i+1)}$ and $d_{\alpha N(i,i+1)}$, as shown in Figure 3 (Marion et al., 1989b). Many of these stretches were assigned to sequence-specific positions on the basis of the known primary structure. However, a substantial number of the amide ^1H/^{15}N chemical shift pairs failed to make connections with any other pairs, because of a lack of matching $^{13}C_{\alpha/\beta}$ or $^1H_\alpha$ chemical shifts or errors in those chemical shifts. This was due to severe overlap in the amide ^1H/^{15}N frequencies and to overlap of aliphatic resonances in the 3D spectra. Therefore, it was necessary to manually inspect the overlapping regions of the 3D data set to discriminate and accurately identify the overlapping components. This iterative analysis successfully yielded complete backbone ^1H, ^{13}C, and ^{15}N assignments for recoverin.

Figure 2A illustrates how residues E136 and D137 are sequentially assigned by these triple-resonance 3D data. The CBCA(CO)NH data for residue D137 indicate that residue E136 must have $^{13}C_\alpha$ and $^{13}C_\beta$ chemical shifts at 58.64 and 28.65 ppm, respectively, which match the $^{13}C_\alpha$ and $^{13}C_\beta$ values determined independently by HNCACB for residue E136. The $^{13}C_\alpha$ and $^{13}C_\beta$ chemical shifts of D137 are found to be 56.05 and 40.26 ppm, respectively, by HNCACB (Figure 2A) which match the $^{13}C_\alpha$ and $^{13}C_\beta$ values determined independently by the CBCA(CO)NH data for the following residue (T138). A total of 155 linkages were obtained from the combined analysis of HNCACB (and/or HNCA) and CBCA(CO)NH data (see Table 1) and represent approximately 80% of the total number of possible linkages. The HNCA experiments yielded a better signal-to-noise ratio than the HNCACB experiment, confirmed all of the linkages established by the HNCACB/CBCA(CO)NH analysis, and provided additional linkages through $^{13}C_\alpha$ chemical shifts only.

The linkage between E136 and D137 is further supported by the sequential connectivity of the ^{13}CO resonance observed in HNCO and (HB)CBCACO(CA)HA data. In Figure 2A, the HNCO data for D137 indicate that the previous residue (E136) must have a ^{13}CO chemical shift at 177.69 ppm which matches the ^{13}CO chemical shift determined by (HB)CBCACO(CA)HA for residue E136. Note that the (HB)CBCACO(CA)HA data also provide $^{13}C_\alpha$ and $^{13}C_\beta$ chemical shifts of E136 which match those obtained from the CBCA(CO)NH data for D137 (Figure 2A). A total of 165 carbonyl linkages were obtained from the combined use of the HNCO and (HB)CBCACO(CA)HA data (Table 1). As demonstrated above, this recently developed (HB)CBCACO(CA)-

Table 2: ^{15}N, ^{13}C, ^{13}CO, and ^{1}H Assignments for Myristoylated Recoverin in the Ca^{2+}-Free State[a]

residue	^{15}N	CO	C_α	C_β	residue	^{15}N	CO	C_α	C_β
G2	111.4 (7.57)	173.2	45.9 (3.96, 3.70)		D78	121.5 (8.61)	177.0	53.3 (4.74)	40.6 (3.00)
N3	115.7 (7.63)	175.8	51.3 (4.83)	39.5 (3.19, 3.13)	G79	108.6 (8.84)	174.1	45.5 (4.36, 3.80)	
S4	116.0 (8.80)	175.9	61.4 (4.23)	62.7 (4.10)	T80	111.6 (7.90)	172.8	59.8 (5.23)	72.2 (4.05)
K5	124.1 (8.40)	178.5	58.5 (4.31)	32.0 (1.94, 1.48)	L81	119.6 (9.18)	177.7	– (3.83)	
S6	115.1 (8.12)	176.7	62.8 (4.22)	63.1 (3.71, 3.65)	D82	123.5 (8.90)	175.3	53.4 (4.84)	40.8 (3.24, 2.56)
G7	108.0 (8.26)	174.4	47.0 (4.08, 3.83)		F83	129.0 (9.06)	175.9	61.5 (4.28)	40.5 (3.28, 3.20)
A8	124.8 (8.24)	180.8	55.1 (4.13)	17.7 (1.63)	K84	119.3 (8.73)	178.2	59.9 (3.98)	32.0
L9	119.9 (8.17)		55.0 (4.31)		E85	118.1 (8.00)	178.0	59.6 (3.93)	29.9 (2.38, 2.15)
S10	117.8 (8.81)	175.5	64.5 (4.01)	62.8 (3.90)	Y86	119.5 (7.94)	175.9	61.6 (3.45)	37.5 (2.45)
K11	118.6 (7.80)	177.7	59.9 (3.81)	31.3 (2.05)	V87	119.3 (8.45)	179.6	67.2 (3.28)	31.4 (2.25)
E12	117.1 (7.41)	178.9	58.7 (4.18)	29.8 (1.85)	I88	123.6 (8.63)	177.3	66.1 (4.08)	37.9 (2.05)
I13	121.0 (8.61)	177.5	64.8 (3.70)	41.5 (1.65)	A89	123.6 (8.66)	180.0	55.7 (3.81)	18.0 (1.54)
L14	117.0 (8.60)				L90	120.1 (8.77)	179.3	– (3.81)	
E15	122.3 (7.77)	179.7	59.7 (4.06)	29.0 (2.33, 2.08)	H91	112.6 (7.30)	177.9	60.6 (3.59)	29.0 (2.25)
E16	119.2 (8.29)	177.2	58.1 (4.20)	28.8 (2.30, 2.10)	M92	113.1 (8.65)	177.9	55.9 (4.67)	31.2 (2.80, 2.60)
L17	118.9 (7.57)	176.2	58.0 (4.37)	40.6 (1.84)	T93	108.3 (7.70)	173.6	61.5 (4.82)	69.5 (4.50)
Q18	112.6 (7.92)	175.2	56.8 (4.00)	25.7 (2.47, 2.31)	S94	116.3 (6.98)	173.5	58.3 (4.12)	64.5 (3.92)
L19	120.6 (7.43)		56.5 (4.10)		A95	124.5 (8.41)	177.5	52.0 (4.36)	18.3 (1.35)
N20	121.8 (8.36)	175.4	53.6 (4.61)	39.3 (2.80, 2.65)	G96	107.8 (8.16)	172.7	44.7 (4.01, 3.86)	
T21	117.4 (8.37)	174.3	61.6 (4.47)	69.8 (4.25)	K97	119.3 (8.83)		56.3 (4.26)	
K22	122.4 (8.23)	176.9	56.4 (4.17)	32.3	T98		175.5	67.5 (3.68)	68.0 (4.02)
F23	118.7 (7.36)	176.0	57.3 (4.82)	40.2 (3.09, 2.82)	N99	117.4 (8.81)	176.4	57.5 (4.10)	36.5 (2.75)
T24	114.5 (8.93)	174.8	60.2 (4.51)	71.1 (4.82)	Q100	119.3 (7.72)	178.0	59.4 (4.22)	28.0 (2.25, 1.97)
E25	120.3 (9.80)	177.7	60.2 (3.89)	28.1 (2.10)	K101	119.9 (8.16)	178.1	60.3 (4.07)	32.2 (2.10)
E26	119.2 (8.34)	178.9	58.9 (4.19)	28.9 (2.26, 2.09)	L102	118.0 (7.86)	178.3	60.5 (4.32)	
E27	121.6 (7.88)	179.6	58.5 (4.13)	29.7 (2.45)	E103	119.9 (8.28)	179.3	59.6 (4.02)	29.8 (2.23)
L28	120.7 (8.42)	177.2	58.4 (4.18)	37.5	W104	122.5 (9.13)	177.7	62.3 (3.86)	28.2 (3.69, 3.25)
S29	112.2 (7.67)	177.0	61.0 (4.59)	62.6 (3.85)	A105	123.6 (8.88)	177.6	54.9 (3.48)	16.7 (1.91)
S30	117.1 (8.55)	177.3	61.4 (4.27)	62.7 (4.10, 4.04)	F106	115.2 (8.16)	177.5	62.0 (3.60)	39.1 (3.29, 3.12)
W31	124.2 (8.66)	177.7	62.4 (4.13)	27.8 (3.50)	S107	114.3 (8.03)	174.7	60.9 (4.10)	62.6 (3.92)
Y32	121.9 (8.40)	176.3	61.9 (3.67)	39.2 (3.33)	L108	123.1 (7.19)		61.0 (3.41)	
Q33	115.8 (8.37)	179.3	58.6 (3.83)	28.2 (2.80, 2.65)	Y109	113.8 (6.72)	176.2	58.5 (4.21)	39.0 (3.07, 2.21)
S34	116.1 (7.99)	175.5	61.4 (4.10)	62.5 (3.85)	D110	123.3 (7.52)	177.1	52.9 (4.95)	39.4 (2.16)
F35	126.5 (8.23)	176.6	60.7 (3.77)	37.8 (2.35, 1.87)	V111	120.0 (7.88)	176.9	63.5 (3.92)	31.7 (2.14)
L36	117.5 (7.59)	179.2	56.0 (3.64)		D112	119.3 (8.55)	176.6	53.7 (4.76)	41.0 (2.82, 2.71)
K37	117.0 (7.09)	177.9	57.9 (3.96)	32.0 (2.98, 1.85)	G113	108.7 (7.75)	175.2	46.2 (3.97, 3.89)	
E38	117.7 (7.42)	176.0	56.6 (4.10)	29.7 (2.00, 1.83)	N114	119.1 (8.67)	176.7	53.8 (4.69)	38.9 (2.91)
C39	120.7 (7.79)	172.0	55.3 (4.67)	25.5 (3.04, 2.10)	G115	110.6 (9.96)	174.5	46.2 (4.12)	
P40		178.5	64.2 (4.44)	31.2 (2.31, 1.93)	T116	109.1 (7.48)	172.6	58.8 (5.60)	72.9 (4.05)
S41	113.1 (8.50)	175.8	58.8 (4.37)	63.7 (4.05)	I117	117.0 (8.88)	172.9	59.7 (4.59)	41.2 (1.42)
G42	111.0 (8.21)	172.3	45.8 (4.42, 3.82)		S118	121.4 (8.80)	174.1	56.6 (5.03)	66.6 (4.25, 3.85)
R43	120.8 (7.73)	175.1	55.0 (5.36)	31.0 (1.75, 1.62)	K119	124.2 (8.58)	177.5	59.4 (2.64)	31.3 (1.06)
I44	116.7 (8.84)	175.1	58.5 (5.12)	42.0 (2.30)	N120	114.9 (8.04)	177.1	55.5 (4.16)	37.2 (2.57)
T45	112.1 (8.93)	175.9	60.3 (4.88)	71.6 (4.88)	E121	122.0 (7.14)	177.3	59.6 (3.54)	27.6 (1.95)
R46	120.3 (8.44)	178.0	59.8 (3.92)	29.6 (1.80, 1.65)	V122	119.0 (7.45)	177.7	67.1 (3.48)	30.7 (2.24)
Q47	118.9 (8.48)	178.8	59.2 (4.10)	27.7 (2.18, 2.07)	L123	119.6 (8.41)	179.2	– (3.91)	
E48	121.7 (7.85)	179.0	58.9 (4.09)	29.6 (2.45)	E124	124.4 (7.78)	178.8	60.5 (4.02)	28.8 (2.30)
F49	120.1 (8.81)	176.0	61.8 (3.84)	38.5 (3.25)	I125	120.6 (7.74)	177.2	65.7 (3.85)	38.8 (2.15)
Q50	117.6 (8.13)	178.4	58.6 (3.87)	27.7 (2.20)	V126	116.5 (8.59)	178.5	65.8 (3.77)	31.8 (2.30)
T51	117.0 (7.79)	176.2	66.1 (3.92)	68.3 (4.35)	T127	119.1 (8.76)	174.4	68.1 (3.73)	68.7 (4.42)
I52	123.6 (7.82)	177.0	65.1 (3.51)	38.5 (1.65)	A128	123.7 (7.77)	178.2	55.4 (4.08)	18.7 (1.84)
Y53	121.7 (8.77)	177.0	62.3 (3.71)	38.0 (2.80)	I129	112.9 (7.55)	177.9	63.9 (3.61)	37.9 (1.90)
S54	111.3 (7.83)	174.7	60.4 (4.17)	63.2 (3.97)	F130	121.8 (8.40)	177.6	60.5 (3.91)	40.1 (3.28)
K55	121.2 (7.28)	177.2	57.8 (3.88)	31.7 (1.57)	K131	116.3 (7.60)	176.6	57.8 (3.99)	31.9 (1.85)
F56	115.6 (7.07)	174.8	60.4 (3.89)	39.6 (1.95)	M132	114.7 (7.58)	176.1	54.2 (4.36)	31.5 (2.10)
F57	117.2 (8.11)	173.4	53.8 (5.15)	38.2 (2.85, 2.21)	I133	122.4 (7.40)	175.8	61.0 (3.92)	36.9 (1.42)
P58		177.7	64.1 (4.52)	31.8 (2.39, 1.99)	S134	126.1 (9.14)	173.9	56.9 (4.58)	62.5 (4.25, 4.05)
E59	117.9 (8.47)	175.9	55.7 (4.42)	29.1 (2.24, 1.97)	P135		179.3	65.2 (4.37)	31.4 (2.41, 1.96)
A60	123.9 (7.70)	176.6	51.8 (4.35)	19.2 (1.49)	E136	117.5 (8.58)	177.7	58.6 (4.06)	28.7 (2.00)
D61	122.5 (8.34)	175.9	51.5 (4.95)	41.9 (2.86, 2.77)	D137	119.1 (7.82)	179.7	56.1 (4.66)	40.3 (2.84, 2.59)
P62		177.3	64.2 (4.38)	32.1 (2.38, 1.93)	T138	115.4 (8.20)	176.6	65.2 (3.87)	68.2 (4.32)
K63	177.8 (8.36)	176.9	56.6 (4.26)	31.3 (1.92)	K139	119.5 (7.21)	176.3	57.5 (4.13)	31.4 (2.93, 1.67)
A64	122.9 (7.67)	179.4	52.9 (4.25)	18.6 (1.56)	H140	115.0 (7.34)	174.9	54.4 (4.84)	29.8 (3.04)
Y65	122.6 (8.23)	176.8	61.5 (4.31)	38.0 (3.22, 2.64)	L141	121.6 (7.23)	175.4	53.0 (4.58)	38.9 (2.80, 2.65)
A66	118.7 (8.29)	180.2	54.6 (3.92)	18.5 (1.40)	P142		177.7	62.6 (4.47)	31.9 (2.45, 1.90)
Q67	117.9 (7.64)	177.2	57.9 (4.17)	28.0 (2.20, 2.10)	E143	122.7 (8.72)	175.6	58.5 (3.99)	29.1 (2.33, 2.08)
H68	121.5 (7.65)	177.9	59.4 (4.30)	30.0 (3.22, 3.15)	D144	112.9 (8.17)	176.2	53.2 (4.60)	39.4 (2.95, 2.65)
V69	119.4 (7.97)	177.3	65.9 (3.44)	31.5 (1.70)	E145	114.5 (7.98)	176.1	54.2 (4.56)	31.4 (2.21)
F70	119.4 (7.68)	176.3	61.2 (3.97)	38.0 (2.28, 2.20)	N146	118.1 (7.35)	173.5	53.4 (4.77)	37.5
R71	118.9 (8.16)	178.2	58.4 (3.85)	30.0 (1.92)	T147	106.3 (7.11)	172.6	57.8 (4.41)	70.2 (3.87)
S72	114.9 (7.66)	174.8	61.0 (4.22)	63.1 (3.82, 3.75)	P148		176.9	65.0 (3.66)	32.1 (1.84, 2.14)
F73	120.8 (7.84)	176.6	59.8 (4.23)	39.5 (2.97)	E149	117.8 (8.86)	179.1	60.6 (3.77)	28.3 (1.84, 1.98)
D74	121.2 (8.28)	176.8	54.4 (4.48)	41.0 (2.45)	K150	119.6 (7.69)	179.9	59.4 (3.98)	33.4
A75	122.6 (7.75)	177.8	53.3 (4.19)	18.5 (1.40)	R151	118.6 (7.78)	177.4	60.2 (3.91)	31.3
N76	115.9 (8.22)	175.1	52.8 (4.91)	38.5 (2.98, 2.78)	A152	120.7 (8.76)	178.5	55.1 (4.06)	17.5 (1.39)
S77	116.2 (8.07)	174.2	58.9 (4.55)	64.1 (4.19, 4.09)	E153	118.0 (7.98)	179.3	58.9 (4.05)	29.1 (2.15)

Table 2 (Continued)

residue	^{15}N	CO	C_α	C_β	residue	^{15}N	CO	C_α	C_β
K154	121.1 (7.93)	178.9	59.2 (3.99)	32.4	N179	117.4 (7.35)	174.0	51.5 (4.89)	39.0 (2.66, 2.44)
I155	119.3 (8.19)	176.4	66.2 (3.63)	38.3 (2.21)	K180	125.0 (8.78)	177.9	58.8 (4.00)	31.6
W156	121.5 (8.72)	179.2	60.8 (4.39)	29.5 (3.43)	E181	118.4 (8.11)	177.5	57.9 (4.11)	28.9 (1.55)
G157	104.3 (8.32)	177.6	46.6 (4.00, 3.90)		I182	117.3 (7.15)	177.6	64.2 (3.63)	37.0 (1.90)
F158	123.5 (8.05)	178.1	59.5 (4.48)	38.3 (3.05, 2.92)	L183	119.3 (7.50)	176.6	– (3.78)	
F159	117.1 (7.75)	176.2	59.4 (4.40)	39.5 (2.94, 2.53)	R184	115.0 (7.60)	177.3	57.9 (4.22)	29.2
G160	109.1 (7.85)	174.4	46.1 (3.90)		L185	118.3 (7.62)		51.7 (4.27)	– (2.14)
K161	118.0 (7.19)	176.2	53.0 (4.52)	33.5 (1.70)	I186	115.8 (7.77)	172.7	60.9 (4.38)	39.6 (1.90)
K162	121.3 (9.20)	178.9	55.1 (4.67)	33.0 (2.10, 1.86)	Q187	115.6 (7.66)	174.0	54.7 (4.51)	30.2 (2.12)
D163	121.7 (8.77)	176.2	57.7 (4.36)	40.5 (2.62)	F188	119.3 (7.93)	173.8	57.0 (4.60)	39.5 (3.04)
D164	115.5 (8.40)	176.0	53.0 (4.75)	39.9 (2.77)	E189	123.8 (7.98)	173.7	53.2 (4.66)	30.3 (1.96, 1.80)
D165	120.6 (7.74)	175.3	54.1 (4.88)	43.4 (3.05, 2.85)	P190		176.7	62.8 (4.33)	31.8 (2.28, 1.93)
K166	118.5 (8.61)	175.2	54.2 (5.05)	35.1 (1.70)	Q191	120.4 (8.57)	176.1	55.8 (4.23)	28.8 (2.08, 2.03)
L167	121.2 (8.81)	177.0	53.0 (4.87)	38.9 (1.54, 1.50)	K192	122.6 (8.22)	176.5	56.3 (4.31)	32.5
T168	113.3 (8.77)	174.5	60.4 (4.99)	71.0 (4.72)	V193	121.5 (7.98)	176.0	62.2 (4.01)	32.1 (2.08)
E169	122.4 (7.69)	177.0	60.0 (2.56)	30.0 (1.65)	K194	124.7 (8.27)	176.5	56.2 (4.23)	32.3 (1.79, 0.94)
K170	117.1 (8.08)	178.6	59.0 (3.93)	32.6 (1.62, 1.36)	E195	122.2 (8.29)	176.3	56.3 (4.21)	30.0
E171	117.2 (7.36)	178.7	58.9 (3.94)	30.5 (2.30)	K196	122.5 (8.26)	176.4	56.0 (4.27)	32.3 (1.79, 1.44)
F172	118.2 (8.44)	176.2	60.6 (4.13)	39.6 (3.00)	L197	123.3 (8.14)	177.2	55.1 (4.31)	42.1 (1.65, 1.58)
I173	118.0 (8.61)	176.5	64.6 (3.58)	38.0 (1.85)	K198	122.3 (8.19)	176.2	56.0 (4.28)	32.4 (1.80)
E174	116.0 (8.18)	180.3	59.2 (3.96)	28.4 (2.47)	E199	122.3 (8.26)	175.8	56.0 (4.25)	30.0 (2.29, 2.00)
G175	107.5 (8.16)	175.9	46.7 (4.14, 3.93)		K200	123.4 (8.28)	175.6	55.9 (4.30)	32.8 (1.83, 1.75)
T176	118.6 (7.30)	175.1	66.6 (3.74)	66.9 (3.90)	K201	124.7 (8.34)	175.0	55.7 (4.36)	32.5 (1.85, 1.78)
L177	116.8 (7.47)	178.2	56.6 (3.87)		L202	130.4 (7.90)		55.9 (4.21)	43.0 (1.60)
A178	117.2 (7.29)	176.9	52.2 (4.28)	19.1 (1.48)					

[a] ^{15}N and ^{13}C chemical shifts are given first, and the attached ^1H chemical shifts are in parentheses. The chemical shift reference used for ^1H and ^{13}C is 3-(trimethylsilyl)propionate, sodium salt. ^{15}N chemical shifts are reported relative to external liquid NH_3.

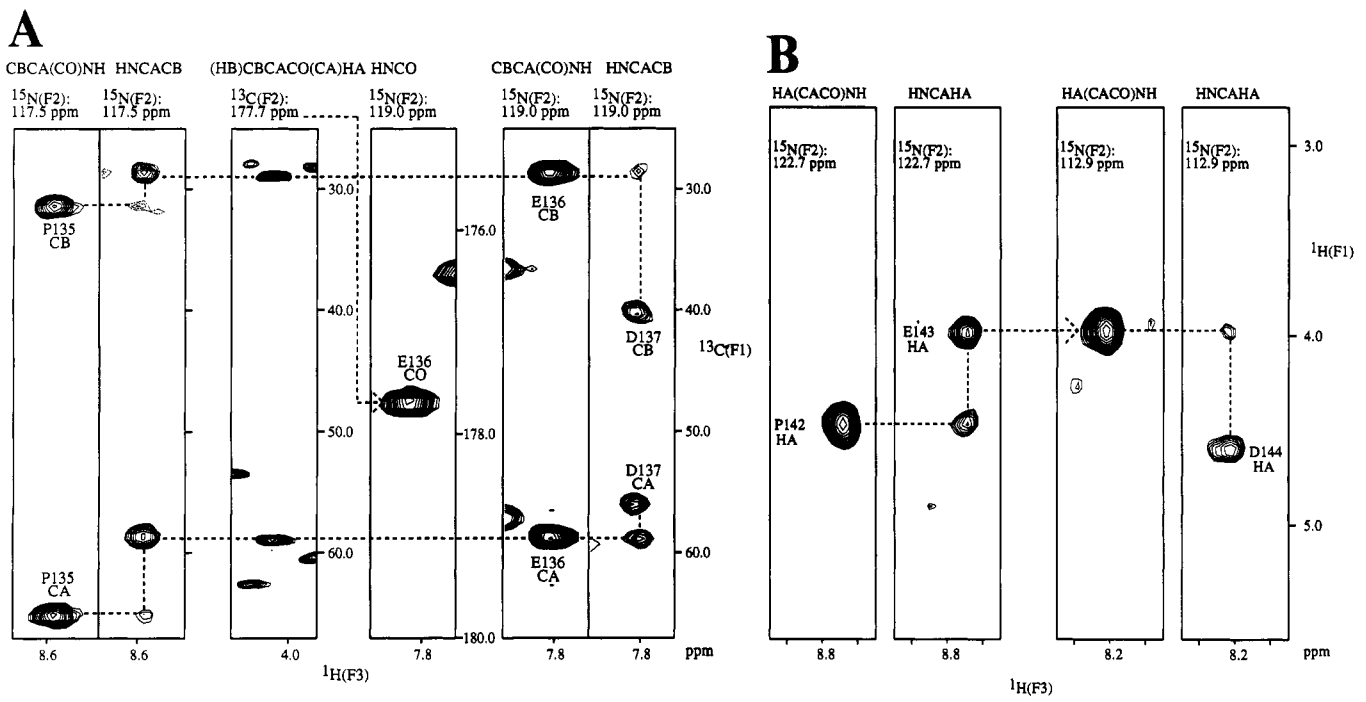

FIGURE 2: (A) Strips of CBCA(CO)NH, HNCACB, (HB)CBCACO(CA)HA, and HNCO spectra showing sequential *J* connectivities of main-chain ^{13}C nuclei for residues P135–D137. (B) Strips of HA(CACO)NH and HNCAHA spectra showing *J* connectivities of H_α resonances for residues P142–D144.

HA experiment was extremely useful for recoverin because it provides four independent chemical shifts, $^{13}C_\alpha$, $^{13}C_\beta$, ^{13}CO, and $^1H_\alpha$, resulting in unambiguous junction points between adjacent residues.

Figure 2B shows how sequential assignments for $^1H_\alpha$ resonances were obtained from the combined use of the HA(CACO)NH and HNCAHA data. The HA(CACO)NH data for residue D144 indicate that the previous residue (E143) must have $^1H_\alpha$ chemical shift at 3.97 ppm. This value matches the $^1H_\alpha$ chemical shift determined by HNCAHA for residue E143 (3.99 ppm). A total of 163 $^1H_\alpha$ linkages were obtained from the combined use of HA(CACO)NH and HNCAHA data (Table 1). As previously noted (Ikura et al., 1991), the HNCAHA experiment correlates the $^{15}N(i)$ and $^1H(i)$ chemical shifts not only with $^1H_\alpha(i)$ but also with $^1H_\alpha(i-1)$ through two-bond coupling. This additional correlation between the amide $^{15}N(i)/^1H(i)$ pair and $^1H_\alpha(i-1)$ provides an independent source of linking $^1H_\alpha(i)$ to $^1H_\alpha(i-1)$, in addition to linkages obtained from the HA(CACO)NH spectra. Finally, the amide ^1H and ^{15}N assignments are depicted in Figure 1 and the NH, ^{15}N, $^1H_\alpha$, $^{13}C_\alpha$, $^1H_\beta$, $^{13}C_\beta$, and ^{13}CO chemical shifts are listed in Table 2.

Secondary Structure. Once the sequential assignments are completed, the secondary structure of the protein could be

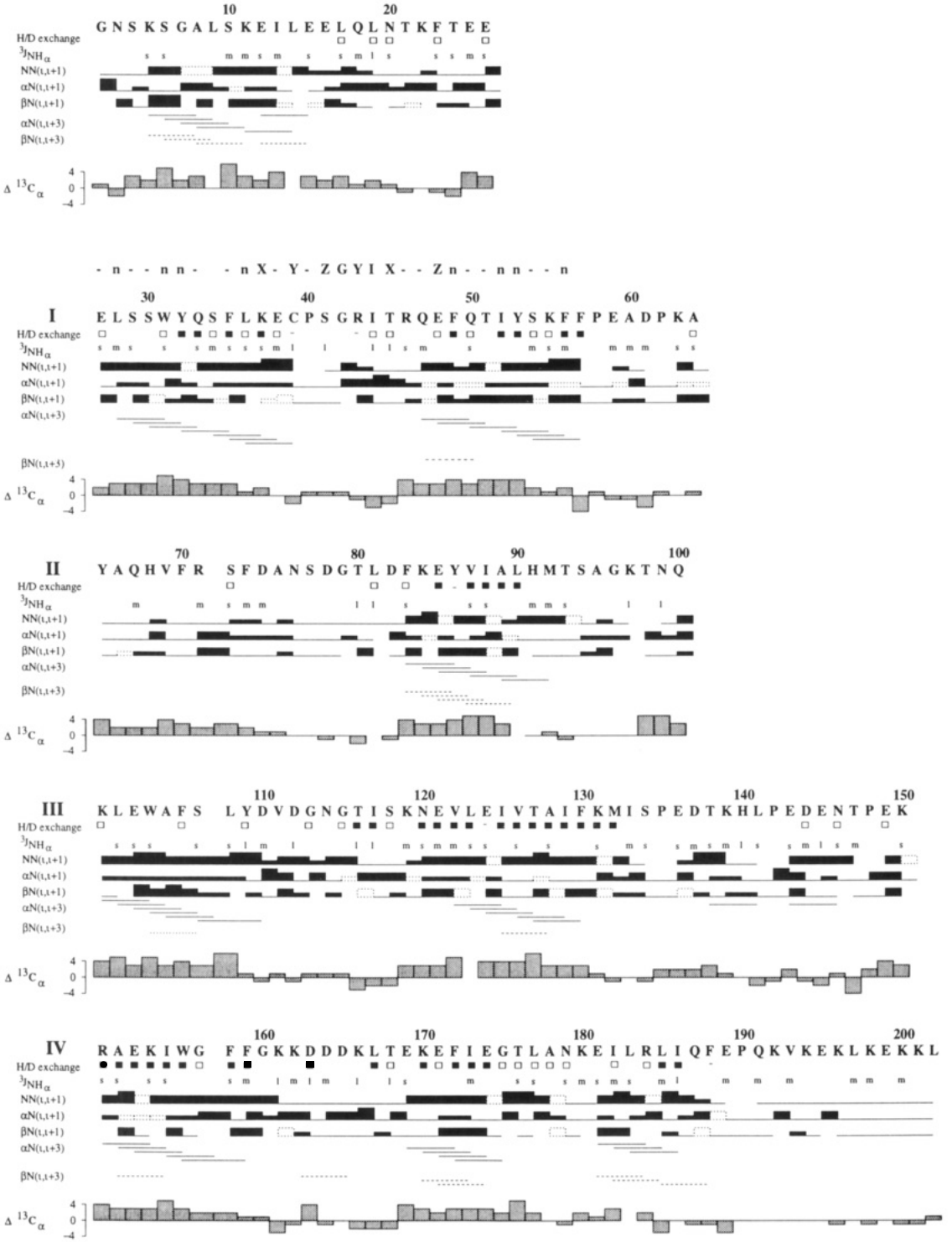

FIGURE 3: Summary of sequential and medium-range NOEs involving NH, H_α, and H_β resonances, amide hydrogen exchange data, $^3J_{NH\alpha}$ coupling, and $^{13}C_\alpha$ secondary shifts observed for Ca^{2+}-free, myristoylated recoverin. The consensus amino acid sequence for EF-hand domain is shown. For amide hydrogen exchange data, residues with slow exchange rates (>4 h) are marked with filled boxes, intermediate exchange rates (1–4 h) are marked with open boxes, and fast exchange rates (<30 min) are unmarked. For the $^3J_{NH\alpha}$ data, large coupling (>8 Hz) is denoted as "l", medium coupling (5–8 Hz) is denoted as "m", and small coupling (<5 Hz) is denoted as "s". NOE connectivities [$d_{NN(i,i+1)}$, $d_{\alpha N(i,i+1)}$, and $d_{\beta N(i,i+1)}$] are represented as strong, medium, weak, or zero intensity in bar graphs. NOEs that are uncertain because of spectral overlap are indicated by unfilled bars.

characterized by NOE connectivity patterns, $^3J_{NH\alpha}$ coupling constants, and amide hydrogen exchange rates (Wuthrich, 1986). In addition, ^{13}C chemical shifts for C_α, C_β, and CO nuclei have been shown to correlate well with the secondary structure of proteins (Spera & Bax, 1991; Wishart et al., 1992). In this study, all of these experimental data have been used to deduce elements of regular secondary structure of myristoylated recoverin.

Figure 3 summarizes amide hydrogen exchange rates, $^3J_{NH\alpha}$ coupling constants, sequential and medium-range NOEs, and $^{13}C_\alpha$ secondary shifts (deviations of $^{13}C_\alpha$ chemical shifts from random coil values) for myristoylated recoverin in the Ca^{2+}-free state. As expected, many residues in Figure 3 are found to possess features that are characteristic of an α-helix: slow amide hydrogen exchange rates, small $^3J_{NH\alpha}$ coupling constants (<5 Hz), strong $d_{NN(i,i+1)}$ and $d_{\alpha N(i,i+3)}$ NOE connec-

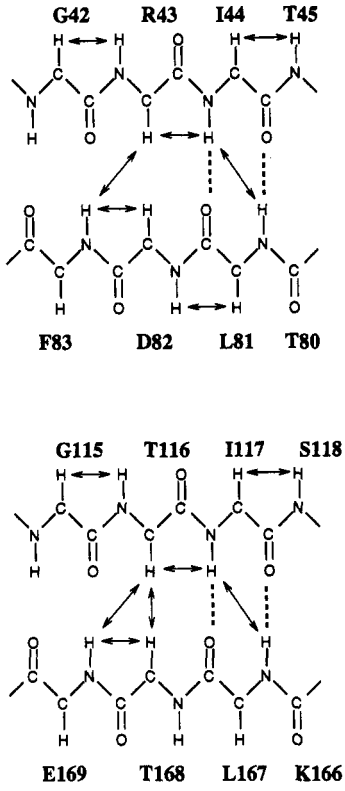

FIGURE 4: Diagram of antiparallel β-sheet regions in Ca^{2+}-free, myristoylated recoverin. Interstrand and sequential backbone NOE connectivities are indicated by the double-headed arrows. Interstrand hydrogen bonds are denoted by the dotted lines.

tivities, and positive $^{13}C_\alpha$ secondary shifts. In addition, residues in helical segments exhibit a positive chemical shift index (Figure 5) using secondary shifts of $^1H_\alpha$, $^{13}C_\alpha$, and ^{13}CO resonances (Wishart et al., 1992; Wishart & Sykes, 1994a,b). Combining all of these results has enabled us to locate 11 α-helix segments, referred to as A to K from the N-terminus in Figure 5: (A) K5–E16, (B) E27–K37, (C) R46–F56, (D) A64–F73, (E) K84–H91, (F) K101–Y109, (G) N120–K131, (H) E136–T138, (I) E149–F159, (J) E169–L177, and (K) E181–R184. Although exact start and finish points of these helices are somewhat uncertain, we have attempted to determine them mainly by the chemical shift index analysis whenever there was uncertainty with NOE connectivities or $^3J_{NH\alpha}$ coupling constants.

Four pairs of helices (B and C, D and E, F and G, I and J) constitute four EF-hand-type helix–loop–helix structural domains (Kretsinger et al., 1986; Moncrief et al., 1990). Helices B, C, E, F, G, I, and J possess the characteristic NMR features of a regular α-helix as described above. The N-terminal helix of EF-2 (helix D), however, exhibits NMR features different from those of the other EF-hand helices. First, the amide protons of the residues in helix D are found to be subject to rapid hydrogen exchange (Figure 3) and give rise to weak intensities in the ^{15}N–^1H HSQC spectrum. Second, $d_{NN(i,i+1)}$ connectivities were weak or absent. Furthermore, $d_{\alpha N(i,i+3)}$ and $d_{\beta N(i,i+3)}$ connectivities could not be observed, most likely because of attenuated intensities of those amide protons. By contrast, the consensus chemical shift index (Figure 5) yielded consecutive positive values in this region, which are indicative of a helical conformation. It should also be noted that the average $\Delta^{13}C_\alpha$ value for residues in helix D (2.6 ppm) is smaller than those of the other EF-hand helices (3.0–3.8 ppm). Finally, the average $^{15}N\{^1H\}$ NOE value for residues in helix D (0.75) is smaller than the corresponding values obtained for the other EF-hand helices (0.81 ± 0.01).

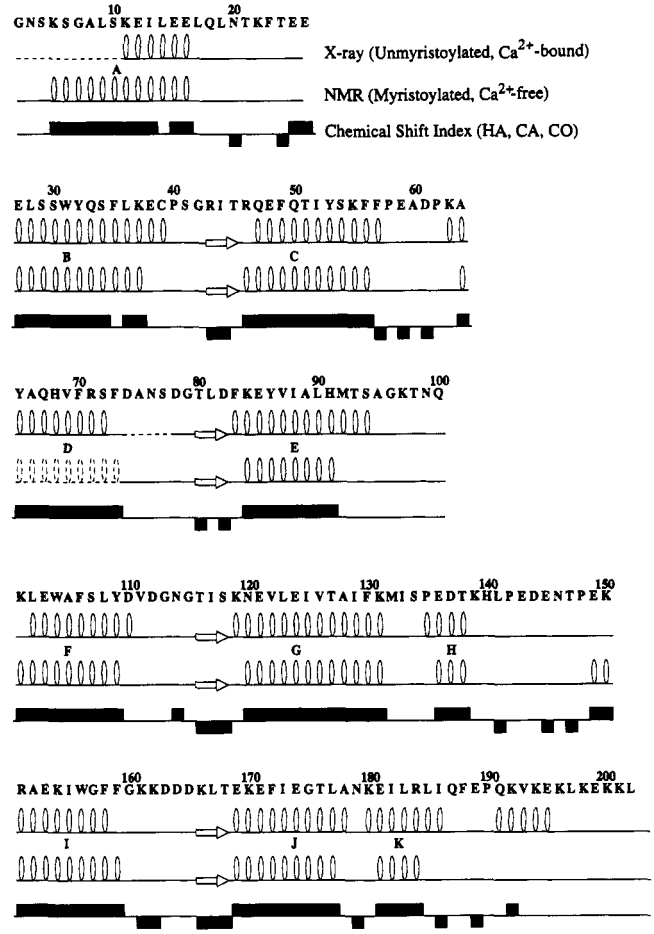

FIGURE 5: Schematic diagram of secondary structure of recoverin and chemical shift index of H_α, C_α, and CO resonances. The NMR structure is obtained for Ca^{2+}-free, myristoylated recoverin. For comparison, the crystal structure of Ca^{2+}-bound unmyristoylated recoverin is also shown. The oval loops indicate α-helices, white arrows indicate β-strands, and solid lines indicate loop and random coil regions. Dashed lines represent disordered regions in the X-ray structure. Dashed ovals indicate that helix D is conformationally flexible. Chemical shift index is calculated from secondary shifts of $^1H_\alpha$, $^{13}C_\alpha$, and ^{13}CO resonances (Wishart et al., 1992).

These results suggest that, in the absence of Ca^{2+}, helix D has a high degree of conformational flexibility compared with the other helices in the four EF-hands.

In addition to the eight EF-hand-type helices, myristoylated recoverin possesses a long N-terminal helix A (K5–E16), a short helix H (E136–T138) between EF-3 and EF-4, and a C-terminal short helix K (E181–R184). Helices A and K are well-defined in terms of consecutive positive values in the consensus chemical shift index (Figure 5) and strong $d_{NN(i,i+1)}$, $d_{\alpha N(i,i+3)}$, and $d_{\beta N(i,i+3)}$ connectivities (Figure 3). However, it should be noted that no slowly exchanging amide protons were found in helix A or H. This may suggest that helices A and H are both exposed to solvent.

Residues within an extended β-type structure are expected to display slow amide hydrogen exchange rates, large $^3J_{NH\alpha}$ coupling constants (>8 Hz), strong $d_{\alpha N(i,i+1)}$ and weak $d_{NN(i,i+1)}$ NOE connectivities, and negative $^{13}C_\alpha$ secondary shifts. These features are observed for residues in the regions R43–T45, T80–D82, T116–S118, and K166–T168 (Figure 3). The negative chemical shift indices using $^1H_\alpha$, $^{13}C_\alpha$, and CO secondary shifts (Figure 5) further support that these regions form an extended backbone conformation. Long-range backbone–backbone NOE connectivities [$d_{NN(44,81)}$, $d_{\alpha N(43,83)}$, $d_{NN(117,167)}$, $d_{\alpha N(116,169)}$, and $d_{\alpha\alpha(116,168)}$] shown by arrows in

Figure 4 indicate that these segments form an antiparallel β-sheet between strands R43–T45 and T80–D82 and between strands T116–S118 and K166–T168. An interstrand NOE between H_α protons of R43 and D82 was expected but could not be seen in the 3D NOESY data set obtained in the present study, suggesting that the β-sheet between strands R43–T45 and T80–D82 may be irregular.

The C-terminal 13 residues (P190–L202) have small secondary chemical shifts for C_α, fast exchanging amide protons, and very weak NOE connectivities (Figure 3). This suggests that this region forms no secondary structure and may be conformationally flexible. Also, the connecting linker between the N- and C-terminal domains contains a region consisting of five residues (T93–K97) which have random coil C_α chemical shifts and fast exchanging amide protons, suggesting that this segment also forms a random coil and/or is conformationally flexible.

DISCUSSION

Recoverin functions as a calcium sensor in vision as a result of translocation to disc membranes by a calcium–myristoyl switch mechanism (Zozulya & Stryer, 1992; Hurley et al., 1993). The binding of calcium ion(s) to recoverin is thought to induce a protein conformational change that leads to extrusion of the N-terminal myristoyl group. The exposed myristoyl group either inserts directly into the lipid bilayer or anchors to another protein associated with the membrane. In the Ca^{2+}-free state, the myristoyl group is thought to become buried inside recoverin, thus preventing recoverin from binding to membranes. Detailed structural information on myristoylated recoverin in both Ca^{2+}-free and Ca^{2+}-bound states is crucial for understanding the molecular mechanism of the calcium–myristoyl switch.

The present NMR analysis on Ca^{2+}-free myristoylated recoverin reveals that the basic architecture comprising four EF-hand motifs and two pairs of antiparallel β-sheets is preserved in the Ca^{2+}-free state. This finding is not surprising since other members of the EF-hand superfamily such as calmodulin (Finn et al., 1993), troponin C (Findlay et al., 1994), and calbindin-D_{9k} (Skelton et al., 1990, 1994) also retain their secondary structure elements in the Ca^{2+}-free state. Among these proteins, calbindin-D_{9k}, consisting of two EF-hand motifs, is the best example for which three-dimensional structures in both Ca^{2+}-free and Ca^{2+}-bound states have been determined by NMR spectroscopy (Kordel et al., 1993). A detailed comparison between the Ca^{2+}-bound and Ca^{2+}-free states of calbindin-D_{9k} indicates that binding of Ca^{2+} induces rearrangement of the helices and consequent exposure of a hydrophobic pocket. Similarly, in recoverin a Ca^{2+}-dependent conformational transition is crucial for transmitting the calcium–myristoyl signal. The present results suggest that the Ca^{2+}-induced conformational change in recoverin may also involve such fine repositionings of the EF-hand helices as observed for other members of the EF-hand superfamily.

Helices in the EF-hand motif vary in length among members of the superfamily. In the case of calmodulin (Babu et al., 1988; Ikura et al., 1991), most of the helices in the four EF-hand domains have a relatively constant length (9–11 residues) except for the N-terminal helix of EF-1 (14 residues) and the C-terminal helix of EF-2 (13 residues). In calcineurin B whose secondary structure has recently been determined by Anglister et al. (1994), larger variations in the helix length have been observed. In the case of Ca^{2+}-free myristoylated recoverin, the most notable difference is in the C-terminal helix of EF-2

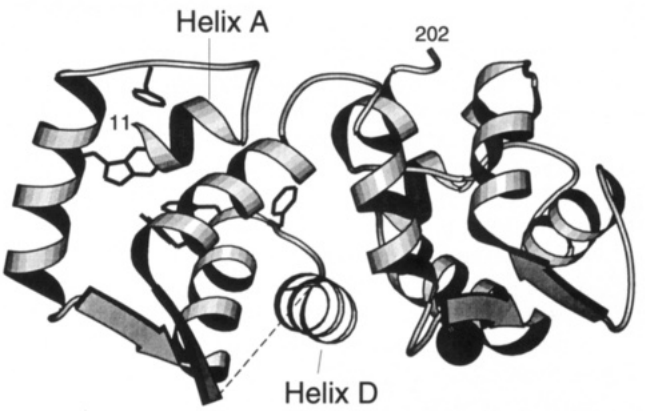

FIGURE 6: Ribbon diagram of X-ray crystal structure of unmyristoylated recoverin with one Ca^{2+} bound (Flaherty et al., 1993). Side-chain atoms are shown for residues Phe-23, Trp-31, Phe-56, Phe-57, and Tyr-86, which together form the hydrophobic groove. A calcium ion bound to EF-3 is shown by a sphere. The dashed line indicates that the main-chain atom positions for residues 74–78 are not known. Helix A in Ca^{2+}-free myristoylated recoverin (residues 5–16) is found to be much longer than in the X-ray structure of unmyristoylated recoverin with one Ca^{2+} bound (K11–E16). Helix D appears to be conformationally flexible in Ca^{2+}-free myristoylated recoverin. The figure was generated with the program Molscript (Kraulis, 1991).

(helix E) which is four residues shorter than the corresponding helix of calmodulin. This difference produces a longer linker (residues 93–100) between the N- and C-terminal domains in recoverin relative to that of calmodulin (residues 78–81). Interestingly, Ca^{2+}-bound unmyristoylated recoverin (Flaherty et al., 1993) has a shorter linker (residues 96–100) than Ca^{2+}-free myristoylated recoverin. The C-terminal helix of EF-3 in recoverin (residues 120–131, helix G in Figure 5) is two residues longer than the corresponding helix of calmodulin. Besides the eight helices in the EF-hand domains, three extra α-helical segments have been identified in Ca^{2+}-free myristoylated recoverin: helix A (residues 5–16), helix H (residues 136–138), and helix K (residues 181–184). These extra helices have also been seen in the crystal structure of the Ca^{2+}-bound unmyristoylated form (Figures 5 and 6) and differentiate recoverin from calmodulin, troponin C, and possibly calcineurin B.

The N-terminal helix of EF-2 (helix D in Figure 5) is found to be a conformationally flexible helix in Ca^{2+}-free, myristoylated recoverin. In the X-ray crystal structure of unmyristoylated recoverin with one Ca^{2+} bound (Flaherty et al., 1993), the corresponding helix has neither notable distortion from regular α-helix nor high B factors. This helix in the crystal structure is packed closely against residues from the helices of EF-3, forming the interface between the N- and C-terminal domains (Figure 6). Close packing between residues of EF-2 and EF-3 partly contributes to the stability of the N-terminal helix of EF-2 in the X-ray structure and thus may account for the difference in length of the domain linker region between the two structures, as described above. The difference in conformational stability seen for the N-terminal helix of EF-2, together with the difference in length of the domain linker region, may have implications for the functional, Ca^{2+}-induced conformational change. We suggest that the binding of Ca^{2+} to EF-3 induces EF-2 to adopt a conformation favorable for the binding of a second Ca^{2+} to recoverin. This may cause the N- and C-terminal domains to come closer together such that the N-terminal helix of EF-2 (helix D) locks into a stable conformation packed against the helices of EF-3 as observed in the X-ray crystal structure (see Figure 6). Small-angle X-ray scattering studies on recoverin (Kataoka et al., 1993) indicate a globular shape for

both the Ca^{2+}-free and Ca^{2+}-bound states with a decrease in the maximum dimension upon Ca^{2+} binding. These data support the idea that Ca^{2+} binding to recoverin causes the N- and C-terminal domains to adopt a more "closed conformation". It should also be noted that a cleft between EF-1 and EF-2 in the N-terminal domain forms an exposed hydrophobic groove in the X-ray structure (Figure 6) which may bind to the myristoyl group. Thus, the N-terminal helix of EF-2 may serve an important role in coupling the binding of Ca^{2+} at EF-3 in the C-terminal domain to the binding of the myristoyl group to the hydrophobic groove in the N-terminal domain.

The long helix located near the N-terminus (helix A in Figure 5) is most likely stabilized by the presence of the myristoyl group in recoverin. This N-terminal helix may help to position the myristoyl group such that it can bind to the exposed hydrophobic groove between EF-1 and EF-2 described above. In the X-ray structure of unmyristoylated recoverin with one Ca^{2+} bound, the N-terminus region (G2–S10) is disordered (Figure 6). Similarly, the N-terminus region in unmyristoylated, Ca^{2+}-free recoverin can be proteolytically cleaved by trypsin, but the myristoylated, Ca^{2+}-free protein is resistant to proteolysis (Dizhoor et al., 1993). These results suggest that the N-terminal helix (K5–E16) in the myristoylated protein may be stabilized indirectly by the interaction of the myristoyl group with the hydrophobic groove between EF-1 and EF-2. Alternatively, the N-terminal helix itself may directly form part of the myristoyl binding pocket. In the X-ray structure of the myristoylated catalytic subunit of cAMP-dependent kinase (Zheng et al., 1993), a similar long, N-terminal helix forms part of a hydrophobic pocket which interacts with the N-terminal myristoyl group.

The ^{1}H, ^{13}C, and ^{15}N backbone assignments presented in this work provide the basis for the determination of the three-dimensional structure of myristoylated recoverin in the Ca^{2+}-free state. Our ultimate goal is to elucidate at atomic resolution the structure of myristoylated recoverin in Ca^{2+}-free and Ca^{2+}-bound states to elucidate the molecular mechanism of the Ca^{2+}–myristoyl switch.

ACKNOWLEDGMENT

We thank L. Kay for help with NMR experiments, F. Delaglio for providing the programs nmrPipe and nmrDraw, D. Garrett for providing the programs Capp and Pipp, T. Harvey for help in coupling constant analysis and for critically reading the manuscript, M. Overduin, A. Crivici, and S. Bagby for critically reading the manuscript, S. Zozulya for help in preparing myristoylated recoverin, and A. Bax for providing us with his manuscript on calcineurin B prior to publication.

REFERENCES

Anglister, J., Grzesiek, S., Wang, A. C., Ren, H., Klee, C. B., & Bax, A. (1994) *Biochemistry 33*, 3540–3547.

Archer, S. J., Vinson, V. K., Pollard, T. D., & Torchia, D. A. (1993) *Biochemistry 32*, 6680–6687.

Babu, Y. S., Bugg, C. E., & Cook, W. J. (1988) *J. Mol. Biol. 204*, 191–204.

Bagby, S., Harvey, T. S., Kay, L. E., Eagle, S. G., Inouye, S., & Ikura, M. (1994) *Biochemistry 33*, 2409–2421.

Bax, A., & Pochapsky, S. (1992) *J. Magn. Reson. 99*, 638–643.

Bax, A., Clore, G. M., & Gronenborn, A. M. (1990) *J. Magn. Reson. 88*, 425–431.

Bodenhausen, G., & Ruben, D. J. (1980) *Chem. Phys. Lett. 69*, 185–189.

Byeon, I.-J. L., Honggao, Y., Edison, A. S., Mooberry, E. S., Abildgaard, F., Markley, J. L., & Tsai, M.-D. (1993) *Biochemistry 32*, 12508–12521.

Dizhoor, A. M., Ray, S., Kumar, S., Niemi, G., Spencer, M., Brolley, D., Walsh, K. A., Philipov, P. P., Hurley, J. B., & Stryer, L. (1991) *Science 251*, 915–918.

Dizhoor, A. M., Ericsson, L. H., Johnson, R. S., Kumar, S., Olshevskaya, E., Zozulya, S., Neubert, T. A., Stryer, L., Hurley, J. B., & Walsh, K. A. (1992) *J. Biol. Chem. 267*, 16033–16036.

Dizhoor, A. M., Chen, C.-K., Olshevskaya, E., Sinelnikova, V. V., Phillipov, P., & Hurley, J. B. (1993) *Science 259*, 829–832.

Findlay, W. A., Sonnichsen, F. D., & Sykes, B. D. (1994) *J. Biol. Chem. 269*, 6773–6778.

Finn, B. E., Drakenberg, T., & Forsen, S. (1993) *FEBS Lett. 336*, 368–374.

Flaherty, K. M., Zozulya, S., Stryer, L., & McKay, D. B. (1993) *Cell 75*, 709–716.

Garrett, D. S., Powers, R., Gronenborn, A. M., & Clore, G. M. (1991) *J. Magn. Reson. 95*, 214–220.

Gray-Keller, M. P., Polans, A. S., Palczewski, K., & Detwiler, P. B. (1993) *Neuron 10*, 523–531.

Grzesiek, S., & Bax, A. (1992) *J. Am .Chem. Soc. 114*, 6291–6293.

Grzesiek, S., & Bax, A. (1993) *J. Biomol. NMR 3*, 185–204.

Herzberg, O., & James, M. N. G. (1988) *J. Mol. Biol. 203*, 761–779.

Howarth, O. W., & Lilley, D. M. J. (1978) *Prog. NMR Spectrosc. 12*, 1–40.

Hurley, J. B., Dizhoor, A. M., Ray, S., & Stryer, L. (1993) *Science 260*, 740.

Ikura, M., Kay, L. E., & Bax, A. (1990) *Biochemistry 29*, 4659–4667.

Ikura, M., Kay, L. E., Krinks, M., & Bax, A. (1991) *Biochemistry 30*, 5498–5504.

Kataoka, M., Mihara, K., & Tokunaga, F. (1993) *J. Biochem. 114*, 535–540.

Kawamura, S. (1993) *Nature 362*, 855–857.

Kawamura, S., Takamatsu, K., & Kitamura, K. (1992) *Biochem. Biophys. Res. Commun. 186*, 411–417.

Kay, L. E. (1993) *J. Am. Chem. Soc. 115*, 2055–2057.

Kay, L. E., & Bax, A. (1990) *J. Magn. Reson. 86*, 110–126.

Kay, L. E., Torchia, D. A., & Bax, A. (1989) *Biochemistry 28*, 8972–8979.

Kay, L. E., Ikura, M., Tschudin, R., & Bax, A. (1990) *J. Magn. Reson. 89*, 496–514.

Kay, L. E., Ikura, M., & Bax, A. (1991) *J. Magn. Reson. 91*, 84–91.

Kay, L. E., Keifer, P., & Saarinen, T. (1992) *J. Am. Chem. Soc. 114*, 10663–10665.

Kay, L. E., Xu, G. Y., Singer, A. U., Muhandiran, D. R., & Forman-Kay, J. D. (1993) *J. Magn. Reson. B 101*, 333–337.

Kobayashi, M., Takamatsu, K., Saitoh, S., Miura, M., & Noguchi, T. (1992) *Biochem. Biophys. Res. Commun. 189*, 511–517.

Kordel, J., Skelton, N., Akke, M., & Chazin, W. J. (1993) *J. Mol. Biol. 231*, 711–734.

Kraulis, P. (1991) *J. Appl. Crystallogr. 24*, 946–950.

Kretsinger, R. H., Rudnick, S. E., & Weissman, L. J. (1986) *J. Inorg. Biochem. 28*, 289–302.

Kuno, T., Kajimoto, Y., Hashimoto, T., Mukai, H., Shirai, Y., Saheki, S., & Tanaka, C. (1992) *Biochem. Biophys. Res. Commun. 184*, 1219–1225.

Lagnado, L., Zozulya, S., Stryer, L., & Baylor, D. A. (1994) in preparation.

Lambrecht, H.-G., & Koch, K.-W. (1991) *EMBO J. 10*, 793–798.

Lenz, S. E., Henschel, Y., Zopf, D., Voss, B., & Gundelfinger, E. D. (1992) *Mol. Brain Res. 15*, 133–140.

Marion, D., Ikura, M., & Bax, A. (1989a) *J. Magn. Reson. 84*, 425–430.

Marion, D., Kay, L. E., Sparks, S. W., Torchia, D. A., & Bax, A. (1989b) *J. Am. Chem. Soc. 111*, 1515–1517.

McPhalen, C. A., Strynadka, N. C., & James, M. N. G. (1991) *Adv. Protein Chem. 42*, 77–144.

Metzler, W. J., Constantine, K. L., Friedrichs, M. S., Bell, A. J., Ernst, E. G., Lavoie, T. B., & Mueller, L. (1993) *Biochemistry 32*, 13818–13829.
Moncrief, N. D., Kretsinger, R. H., & Goodman, M. (1990) *J. Mol. Evol. 30*, 522–562.
Muhandiran, D. R., Farrow, N. A., Xu, G. Y., Smallcombe, S. H., & Kay, L. E. (1993) *J. Magn. Reson. B 102*, 317–321.
Okazaki, K., Watanabe, M., Ando, Y., Hagiwara, M., Terasawa, M., & Hidaka, H. (1992) *Biochem. Biophys. Res. Commun. 185*, 147–153.
Pascal, S. M., Muhandiran, D. R., Yamazaki, T., Forman-Kay, J. D., & Kay, L. E. (1994) *J. Magn. Reson. B 103*, 197–201.
Persechini, A., Moncrief, N. D., & Kretsinger, R. H. (1989) *Trends Neurosci. 12*, 462–467.
Polans, A. S., Buczylko, J., Crabb, J., & Palczewski, K. (1991) *J. Cell Biol. 112*, 981–989.
Pongs, O., Lindemeier, J., Zhu, X. R., Theil, T., Engelkamp, D., Krah-Jentgens, I., Lambrecht, H.-G., Koch, K. W., Schwemer, J., Rivosecchi, R., Mallart, A., Galceran, J., Canal, I., Barbas, J. A., & Ferrus, A. (1993) *Neuron 11*, 15–28.
Ray, S., Zozulya, S., Niemi, G. A., Flaherty, K. M., Brolley, D., Dizhoor, A. M., McKay, D. B., Hurley, J., & Stryer, L. (1992) *Proc. Natl. Acad. Sci. U.S.A. 89*, 5705–5709.
Resh, M. D. (1994) *Cell 76*, 411–413.
Sambrook, J., Fritsch, E. F., & Maniatis, T. (1989) *Molecular Cloning*, Cold Spring Harbor Laboratory Press, New York, NY.
Skelton, N. J., Kordel, J., Forsen, S., & Chazin, W. J. (1990) *J. Mol. Biol. 213*, 593–598.
Skelton, N. J., Kordel, J., Akke, M., Forsen, S., & Chazin, W. J. (1994) *Nature Struct. Biol. 1*, 239–245.
Spera, S., & Bax, A. (1991) *J. Am. Chem. Soc. 113*, 5490–5492.
Strynadka, N. C., & James, M. N. G. (1989) *Annu. Rev. Biochem. 58*, 951–998.
Takamatsu, K., Kitamura, K., & Noguchi, T. (1992) *Biochem. Biophys. Res. Commun. 183*, 245–251.
Terasawa, M., Nakano, A., Kobayashi, R., & Hidaka, H. (1992) *J. Biol. Chem. 267*, 19596–19599.
Wishart, D. S., & Sykes, B. D. (1994a) *J. Biomol. NMR 4*, 171–180.
Wishart, D. S., & Sykes, B. D. (1994b) *Methods Enzymol.* (in press).
Wishart, D. S., Sykes, B. D., & Richards, F. M. (1992) *Biochemistry 31*, 1647–1651.
Wittekind, M., & Mueller, L. (1993) *J. Magn. Reson. 101*, 201–205.
Wuthrich, K. (1986) *NMR of Proteins and Nucleic Acids*, John Wiley & Sons, Inc., New York, NY.
Yamagata, K., Goto, K., Kuo, C.-H., Kondo, H., & Miki, N. (1990) *Neuron 2*, 469–476.
Zheng, J., Knighton, D. R., Xuong, N.-H., Taylor, S. S., Sowadski, J. M., & Ten Eyck, L. F. (1993) *Protein Sci. 2*, 1559–1573.
Zozulya, S., & Stryer, L. (1992) *Proc. Natl. Acad. Sci. U.S.A. 89*, 11569–11573.
Zuiderweg, E. R. P., & Fesik, S. W. (1989) *Biochemistry 28*, 2387–2391.